SYNTHESIS OF MAGNETITE NANOPARTICLES AND EXPLORING THEIR APPLICATION IN THE REMOVAL OF Pt^{2+} AND Au^{3+} IONS FROM AQUEOUS SOLUTIONS

Liliana Giraldo[a] and Juan Carlos Moreno-Piraján[b]*

This investigation studies the adsorption of Pt^{2+} and Au^{3+} ions from nitrate solutions using nanoparticles of magnetite (Fe$_3$O$_4$) synthesized in this work. The study is carried out by the analysis of the adsorption of Pt^{2+} and Au^{3+} ions on the surface of the nanoparticles by modifying several variables: contact time, solution pH, and initial Pt^{2+} and Au^{3+} ion concentration. The highly crystalline nature of the magnetite structure with a diameter of around 10 nm was characterized with transmission electron microscopy (TEM) and X-ray diffractometry (XRD). The surface area was determined to be 117.5 m$^2\cdot$g^{-1}. The surface functional groups were investigated with Fourier transform-infrared spectroscopy (FTIR) as well. Batch experiments were carried out to determine the adsorption kinetics and mechanism of Pt^{2+} and Au^{3+} by these magnetite nanoparticles. The adsorption process was found to be pH dependent. The adsorption process better followed the pseudo-second-order equation and Freundlich isotherm. It has been found that the equilibrium can be attained in less than 5 min. Immersion microcalorimetry was explored as a new tool to establish the adsorption capacity of the ions under study with promising results.

* Corresponding Author
    E-Mail: jumoreno@uniandes.edu.co

[a]   Facultad de Ciencias, Departamento de Química, Universidad Nacional de Colombia, Carrera 30 No 45 03, Ciudad Universitaria, Bogotá, Colombia.
[b]   Facultad de Ciencias, Departamento de Química, Grupo de Investigación en Sólidos Porosos y Calorimetría, Universidad de Los Andes, Bogotá, Colombia. Carrera 1 No 18 A 10, Bogotá, Colombia.

Introduction

With the development of industry, humans have tried to improve their quality of life. However, many of these advances have led to major pollution problems worldwide, within which we can mention volatile organic compounds (VOCs) and heavy metal ions. All these elements thrown into water bodies have endangered ecosystems, particularly in developing countries, where despite of controls for these emissions government agencies do not exercise such audits. Industries such as petrochemical, dye, electroplating and the tanneries are big polluters, mainly for the rivers. Today many countries have endangered ecosystems due to this uncontrolled emission of pollutants and many species are on the verge of disappearing. A critical example is the Río Bogotá (Colombia), located on the outskirts of this South American capital, which is one of the most polluted in the world due to electroplating and tanneries endanger for the river. Furthermore, Colombia is a mining country, and it has minerals such as gold, platinum, iridium and others, which are exploited irrationally, generating more pollution for the environment[1-5].

Significant global solutions have been created to remove these pollutants: among them we can mention biological systems, widely used and with some success, while other systems used include porous solids because of their wide variety, and their characteristics have been extremely useful. The removal of ions such as chromium, mercury, zinc and others is carried out by activated carbon, zeolites, and mesoporous solids, to name a few[7-12]. Other systems for removing contaminants are systems through membranes, and some less used such as precipitation systems. Nanoparticles with magnetic properties have recently been explored through adsorption systems and these enable the adsorption of metal ions and can realize major disposal thereof. Today this continues to be explored in this direction with these materials that are very new, not only in the synthesis of the same but in the conditions under which they can operate to achieve a better adsorption of metal ions, which are now one of the major global problems. The key potential impact areas for nanotechnology in water treatment applications can be divided into three groups, namely treatment and remediation, sensing and detection, and pollution control[13,14].

In this study, magnetite nanoparticles were synthesized following literature protocols[15] and their efficiency in the removal of Pt^{2+} and Au^{3+} ions were investigated. This is done through studies of adsorption capacity, kinetic effect of pH and the effect of contact time. Work plus calorimetry tests were conducted to explore this immersion technique in these investigations and whether this technique can be used for monitoring the adsorption of the ions being studied.

Experimental

Preparation and characterization of magnetite nanoparticles

In this work, magnetite nanoparticles were prepared according to published procedures in the scientific literature[15-17]. The method of co-precipitation, from aqueous solutions of Fe^{3+} and Fe^{2+} salts by addition of bases in an inert atmosphere at room temperature, is suitable for the synthesis of magnetite nanoparticles. The synthesis of magnetite nanoparticles can be represented by the overall reaction equation given below:

$$2\ FeCl_3 + FeCl_2 + 8\ NH_3 + 4\ H_2O \rightarrow Fe_3O_4 + 8\ NH_4Cl$$
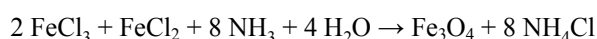
We adjusted the amounts of each of the reagents according to our reagents and equipment available. For the synthesis, a 1.5 M ferric chloride hexahydrate and a 2.5 M ferrous chloride tetrahydrate solution was prepared, and then 4.5 mL of FeCl$_2$·4H$_2$O and 20 mL of FeCl$_3$·6H$_2$O solutions were added to a flask. The mixture was stirred with a stirring speed of 400 rpm at a temperature of 250 °C, and the alkaline solution was added at a rate of 0.9 mL min^{-1} from a burette with controlled speed through an automatic titrator. Several washings of the obtained solution were performed with methanol and water in a ratio of 50:50. Finally, nanoparticles were obtained by lyophilization treatment. A schematic showing the assembly used is shown in Figure 1.
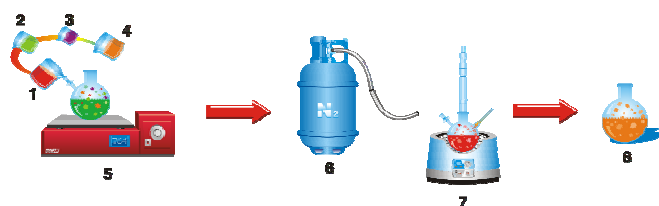

Figure 1. Synthesis equipment for producing magnetite nanoparticles: 1 FeCl$_3$, 2 FeCl$_2$, 3 NH$_3$, 4 H$_2$O, 5 reactor, 6) nitrogen, 7 heating mantle, 8 products.

Characterizations of magnetite nanoparticles

X-ray diffraction (XRD) patterns of the produced nanoparticles were recorded on a Rigaku Rotaflex X-ray diffractometer using Cu Kα radiation. The X-ray tube current was 100 mA with a tube voltage of 40 kV. The 2θ angular regions between 20 and 70° were examined at a scan rate of 0.1° min^{-1}. The determination of the morphology and size of magnetite nanoparticles was performed by transmission electron microscopy (TEM) and was carried out on a JEOL (JEM 3100 F, Japan) microscope at 200 kV. The IR spectra of the magnetic powders in KBr pellets were recorded with a Thermo Nicolet NEXUS 670 spectro-photometer in the 4000-400 cm^{-1} range. The magnetization curves were recorded at room temperature using a vibrating sample magnetometer (VSM) characterized with a Lake Shore 7400 series VSM. Specific (BET) and external nanoparticle surface areas were measured by nitrogen adsorption and desorption at 77 K, using an Autosorb 3B (Quantachrome, MI, FL, USA) analyzer. The samples were degassed at 150 °C under N$_2$ flow overnight before analysis. Surface area was calculated using the BET equation. The

total pore volume, V$_{pore}$, was evaluated from nitrogen uptake at a relative pressure of ca. 0.97, using the adsorption branch. N$_2$ adsorption measurements were performed in duplicate to check the proper functioning of the equipment and the entire technique, and the average values have been presented[18,19].

Adsorption and desorption studies

The adsorption of Pt^{2+} and Au^{3+} ions by the magnetite nanoparticles was investigated in an aqueous solution at 25 °C. In general, the magnetite nanoparticles (5.0 mg) were put into 50.0 mL of aqueous solution containing Pt^{2+} and Au^{3+} ions (100 mgL^{-1}), the mixture was adjusted to a certain pH with NaOH or HCl and mixed by ultrasonication for several minutes until the equilibrium was established. For removal of Pt^{2+} and Au^{3+} ions from water, these were separated from the mixture with a permanent handheld magnet. The concentration of Pt^{2+} and Au^{3+} ions in the supernatant was measured by flame atomic absorption spectrometer (Ruili WFX-130).[20-23]

Tests of pH, temperature, and time effects

Tests aimed for the analysis of the pH effect were conducted at 25 °C and the initial pH of the solution was adjusted without a significant change in the initial concentration of metal ions in the solution. Standard 0.1 M HCl and 0.1 M NaOH solutions were used for pH adjustment. The effect of temperature and time was investigated as well, and adsorption tests were carried out between 15 °C and 45 °C. When adsorption equilibrium was reached, the nano-adsorbent was conveniently separated via external magnetic field and the solution was filtered to allow metal concentration measurements[21-25].

Kinetic studies

For the adsorption kinetic studies, the metal ion initial concentration was set to 25 mg L^{-1} for each metal, and the experiments were carried out in a temperature incubator at 298 K, 300 rpm, and in a solution with a pH of 6.5. In order to determine the time required to reach the adsorption equilibrium, samples were analyzed for metal ion concentration at predetermined time intervals. To assure the accuracy, reliability, and reproducibility of the collected data, all batch tests were performed in triplicate and only average values were reported. Blank tests were run in parallel on metal solutions without addition of sorbent, showing that the experimental procedure does not lead to any reduction of metal concentration and pH variation unrelated to sorbent effects[23,24].

For all the tests, the concentration of metal ions in the supernatant was measured by a plasma-atomic emission spectrometer (ICP-AMS, Optima 3000XL, PerkinElmer).

Immersion calorimetry studies

In order to explore whether the immersion enthalpies between synthesized nanoparticles and aqueous solutions of Pt^{2+} and Au^{3+} ions at a concentration in a range between 10 and 100 mg L^{-1}, a series of calorimetric measurements were

carried out using a microcalorimeter local building immersion reported in the literature[26]. A microcalorimeter schematic is presented in Figure 2. The equipment comprises a thermoelectric system consisting of four thermopiles, which gives a high sensitivity. These thermocouples are embedded in an aluminium block which comes without leaving any dead space and thus avoids false electrical contacts. At the centre of the aluminium block, there is a hole built by EDM, where it enters a cell in special stainless steel, with a capacity of 10 mL, and that likewise leaves no space this time to avoid bad thermal contacts. The aluminium block, or heat reservoir, is placed within a teflon joint which soon stabilizes the temperature. The teflon block has electrical connections for the sensors and electrical resistance, which is used for electric calibrations. On the inside of the microcalorimeter lid is also placed the vial holder system containing the adsorbent.

The measurement is carried out by accurately weighing milligram, 0.10 grams of magnetite, which is degassed under high vacuum to remove impurities having adhered at 90 °C for 6 hours. Once this procedure is suspended in the vacuum, we remove the heating mantle, and proceed to seal the glass ampoule. Then it is placed on the inner lid of the calorimeter, the calibration resistor is connected and the microcalorimeter is closed and we proceed to capture data using software developed in our laboratory, until the baseline stabilizes. Once this is done the ampoule is broken to produce the wetting between the magnetite and the respective solution of Pt^{2+} and Au^{3+} ions (Figure 2). These steps are performed for a range of concentrations between 10 mg L^{-1} and 100 mg L^{-1} for each ion. Once thermal equilibrium is re-established, it is expected that the time corresponding to equilibrate the thermometric signal is performed again and the corresponding electrical calibration finalized with each measurement. For each experiment five replicates were conducted for statistical processing.
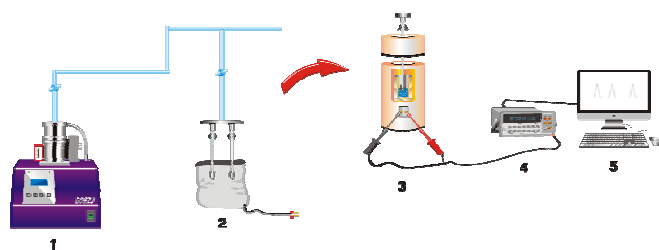

Figure 2. Set-up of microcalorimeter for immersion determinations: 1. Vacuum pump, 2. Desorption system, 3. Microcalorimeter complete, 4. Multimeter, 5. Computer.

Result and discussion

Particle characterization

Magnetite nanoparticles were characterized by XRD results as shown in Figure 3. Recorded peaks are characterized by well defined and there are no extraneous peaks, which shows that there is purity and crystallinity of the particles obtained, and the results of this study are consistent with those reported for magnetite in the literature.

Average size was determined using crystal Scherrer equation 1[27]. To search for the particle size the most intense peak is chosen, which in this case is found to be approximately 2θ = 35.55 with κ = 0.9, λ = 0.1540598 nm, FWHM = β

$$MC\Delta = \frac{\kappa\lambda}{\beta\cos\theta}\frac{180}{\pi} \qquad (1)$$

The strong and sharp peaks suggested that Fe_3O_4 crystals are highly crystalline. However, the broadening in the reflection peaks was due to the particles' size at the nano domain. All XRD patterns show a diffraction peak at 2θ = 35.70° which corresponds to the spinel phase of Fe_3O_4 nanoparticles. The XRD peaks of magnetic nanoparticles at 2θ = 30.22°, 43.52°, 57.43° and 63.11° were found to be in good agreement with those of previously reported 2θ values of Fe_3O_4 nanoparticles and match well with the JCPDS Card No.19-0629. The average crystallite size of nanoparticles was calculated from the lower full width at half maximum (FWHM) of (3 1 1) diffraction reflection using Scherrer's equation: D = 0.9λ/β cos θ , where D is the particle size, λ is the X-ray wavelength (nm), θ is Bragg's angle; β is the excess line broadening (radiant), and the particle size of Fe_3O_4 nanoparticles was found in the range of 20–25 nm using Scherrer's equation. The intensity of all diffraction peaks at 2θ = 35.70° are followed by the decreasing of intensity due to formulation of more crystalline phase particles in all annealed Fe_3O_4 nanoparticles. The estimated particle size at 300 °C was estimated as ~21 nm[28-31].
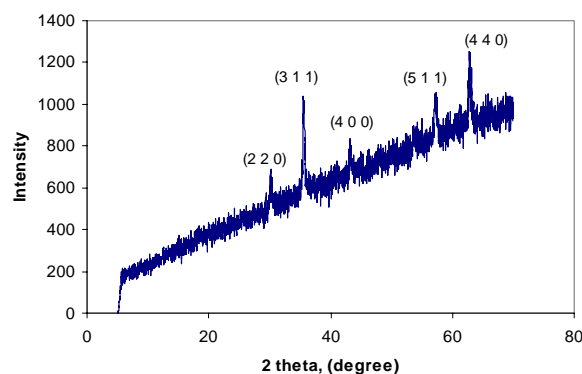

Figure 3. XRD of synthesized magnetite nanoparticles.

Figure 4 shows a transmission electron micrograph. This sample and homogeneous particles are of uniform size. The TEM image of synthesized nanoparticles reveals no presence of contaminants; this is a very important development in this research since it is necessary to have pure particles for analysis of the adsorption capacity of the ion under study. The relative size of the particles is about ~21 nm.

When performing the infrared spectrum analysis of the magnetite nanoparticles, it can be seen that the actual spectrum shows well-defined bands, confirming that particles have been obtained in a purity suitable for the present study. The spectrum shows characteristic bands between the analysed range of 4000-500 cm⁻¹. In Figure 5, the peak at ~3500 cm⁻¹ is attributed to the stretching vibrations of -OH, which is assigned to OH⁻ absorbed by

Fe_3O_4 nanoparticles, and the peak at ~584.3 cm^{-1} is attributed to the Fe-O bond vibration of Fe_3O_4[31].

The isotherm of nitrogen adsorption (data not shown) of the particles exhibit a specific surface area measured by BET method was 117.5 m^2 g^{-1}.
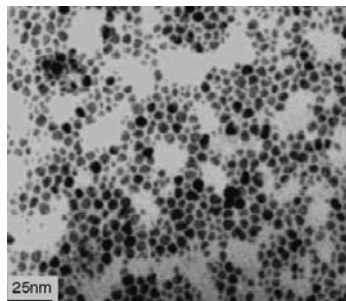

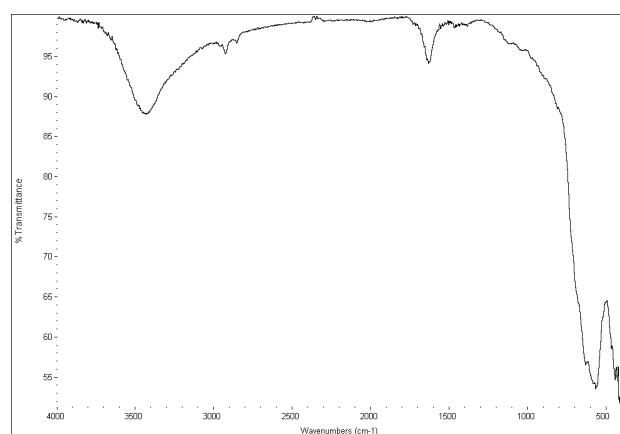**Figure 4**. TEM image of synthesized magnetite nanoparticles.

Figure 5. FTIR of synthesized magnetite nanoparticles.

Vibrating sample magnetometer (VSM) studies

Figure 6 shows the plot of the magnetization 'M' versus applied field 'H' (between −2000 Oe and +2000 Oe) of the prepared Fe_3O_4 nanoparticles obtained.
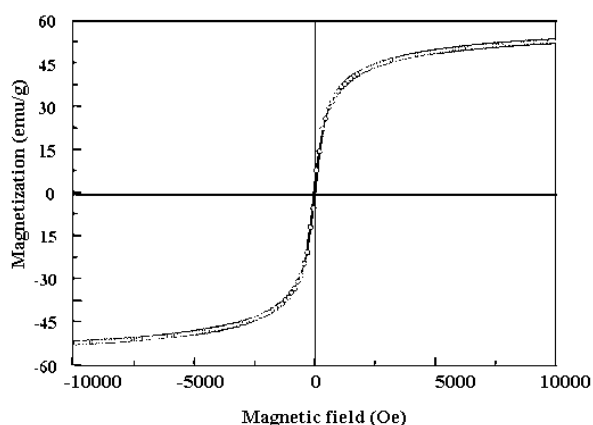

Figure 6. Magnetization curves of synthesized magnetite nanoparticles.

The VSM curve reveals the formation of a hysteresis loop for the Fe_3O_4 nanoparticles, with zero coercivity and remanance values, which exhibits superparamagnetic behaviour of Fe_3O_4 nanoparticles. On increasing the applied field from 0 to 1000 Oe, the magnetization 'M' increases sharply, and becomes nearly saturated at about 1000 Oe. It was found that all the samples of the magnetite have strong magnetic responses to a varying magnetic field. The hysteresis loops showed smooth change of magnetization with the applied field. This was reported in the literature[32,33].

Effect of pH

The pH of the aqueous solution is an important controlling parameter in heavy metal ion adsorption processes, as reported by several authors in the literature. Figure 7 shows the effect of a pH solution in the range 2-12 on the removal of Pt^{2+} and Au^{3+} ions from aqueous solutions by magnetite nanoparticles. As a matter of fact, at higher pH the determination of reliable adsorption capacity is not possible, due to the possible precipitation of cations as hydroxides.
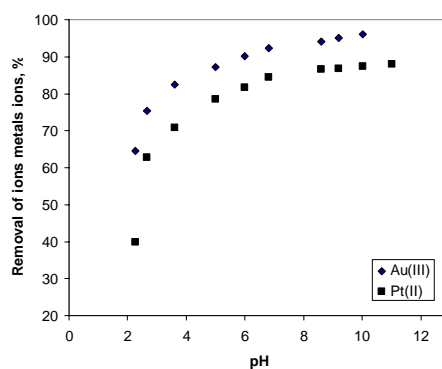

Figure 7. The effect of pH on the adsorption of Pt^{2+} and Au^{3+} ions onto magnetic Fe_3O_4 nanoparticles. T = 298 K, t = 6 h, adsorbent dosage = 50 mg, $V_{solution}$= 50 mL, initial metal ion concentration =25 mg·L^{-1}.

Experiments were carried out at 25 °C with a contact time of 6 h. The adsorption efficiency increases by increasing the pH, for all the investigated cations. As an example, Au^{3+} adsorption efficiency gradually increases from 65.7% to 94.5% when the pH increases from 2 to 6.5.

The results demonstrate that the removal of the cations was mainly dependent on the proton concentration in the solution. This has been previously attributed to the formation of surface complexes between the functional groups ($\equiv$FeOH) of the sorbent and, for example, the Au^{3+}ions, with the possible reaction being expressed as follows[34]:

$$s\ H_2O + q\ \equiv\!FeOH + r\ Au^{3+} \leftrightarrow$$
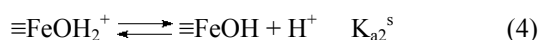$$(\equiv\!FeO)_q Au_r(OH)_s^{(2-q-s)} + (s+q)\ H^+ \qquad (2)$$
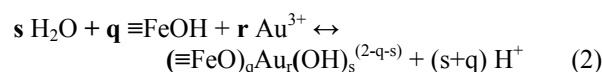
where $(\equiv\!FeO)_q Au_r(OH)_s^{(2-q-s)}$ corresponds to the surface complexes and s, q and r are the stoichiometric coefficients. When pH increases, this equilibrium shifts in such a manner that a greater number of sites are present in the more reactive deprotonated form, thereby leading to a higher uptake of Au^{3+}.

The results show very similar trends for Pt^{2+} adsorption efficiency; this pH dependency has been attributed to the formation of surface complexes similar to those reported for Au^{3+} cations.

Furthermore, from the measured zeta potential of magnetite solution at different pH values, it appears that the magnetite surface has a positive charge at a pH below 6.0 and a negative charge when pH is higher than 6.0[34]. This result is consistent with the experimental data reported in Figure 7.

Furthermore, it should be noted that magnetite is an amphoteric solid, which can develop charges in the protonation (Fe-OH + H^+ ↔ Fe-OH$_2^+$) and deprotonation (Fe-OH ↔ Fe-O$^-$ + H^+) reactions of Fe-OH sites on the surface[35]. The reactions can be written as:

$$\equiv FeOH \rightleftharpoons \equiv FeO^- + H^+ \qquad K_{a1}^s \qquad (3)$$

$$\equiv FeOH_2^+ \rightleftharpoons \equiv FeOH + H^+ \qquad K_{a2}^s \qquad (4)$$

and the corresponding acidity constants as

$$K_{a1}^s = \frac{[H^+]\{\equiv FeO^-\}}{\{\equiv FeO\}} \qquad (5)$$

$$K_{a2}^s = \frac{[H^+]\{\equiv FeOH\}}{\{\equiv FeOH_2^+\}} \qquad (6)$$

where [ ] is the solution species concentration in mol L^{-1} and { } is the solid surface concentration in mol g^{-1}. According to the pH of the solution, the surface is charged differently and could behave as an anion or cation exchanger. It is important to realize that negative, positive and neutral functional groups can coexist on the surface of the magnetite. At pH<pH$_{zpc}$, the FeOH$_2^+$ groups predominate over the FeO$^-$ groups, i.e., although the surface has a net positive charge, some FeO$^-$ groups are still present. At pH$_{zpc}$, the number of FeOH$_2^+$ groups equals the number of FeO$^-$ groups, and as the pH increases, the number of FeO$^-$ groups increases (pH$_{zpc}$ have been calculated but not reported here). It follows that magnetite particles may adsorb either negatively or positively charged species by electrostatic attraction depending on the pH, even if, as previously reported, a complete analysis of all the pH intervals is not possible dealing with cations.

Figure 7 shows that a magnitude of adsorption can be defined according to the following order: $Pt^{2+}<Au^{3+}$. The uptake of Pt^{2+} and Au^{3+} ions onto magnetite nanoparticles occurs by physico-chemical interactions, likely represented by electrostatic attractions. In particular, the size of hydrated ionic radii seems to influence the interactions with the negative-charged adsorption site, as the greater the ion's hydration, the farther it is from the adsorbing surface and the weaker its adsorption (hydrated ionic radii: Pt^{2+}: 0.130 nm < Au^{3+}: 0.099 nm). Hence, Au^{3+} has the lowest hydrated ionic radius and the highest capability to compete with proton and, hence, the highest comparative adsorption capacity.

In the literature, results of the same order of magnitude have been reported than that obtained in this work in terms of metal adsorption capacity on the same sorbents[35].

Although many different sorbents can be used for the same purpose, magnetic nanosorbents possess a number of unique physical and chemical properties and they are easily dispersed in aqueous solutions. A large number of their atoms are superficial atoms, which are unsaturated and, hence, can determine high adsorption capacity towards several metal ions. Magnetic particles can be removed very quickly from a matrix using a magnetic field, but they do not retain their magnetic properties when the field is removed. This system also has several advantages compared with conventional or other nanoadsorbents such as the absence of secondary wastes and the possible recycling of the materials involved on an industrial scale. Furthermore, the magnetic particles can be tailored to separate specific metal species in water, wastes or slurries. However, from a practical point of view, there is a major drawback in the application of such nanomaterials for treating wastewater. Because the treatment of wastewater is usually conducted in a suspension of these nanoparticles, an additional separation step is required to remove them from a large volume of solution, resulting in increased operating costs. This type of system can be implemented in small towns in order to remove these precious metals efficiently and without polluting the ecosystem.

Adsorption isotherms

Adsorption isotherms of Pt^{2+} and Au^{3+} ions on magnetite nanoparticles are reported in Figure 8.
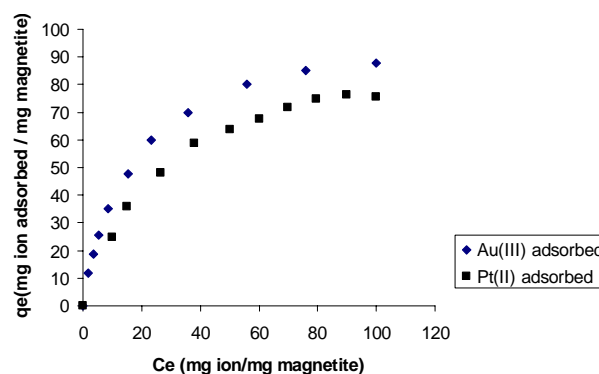

Figure 8. Pt^{2+} and Au^{3+} ions adsorption isotherms on Fe₃O₄ magnetite nanoparticles. T=25 °C, pH=6.5. Comparison between experimental data and Langmuir model. V$_{solution}$= 50 mL, initial metal ion concentration=25 mg·L^{-1}.

Under the above-mentioned conditions, the maximum adsorption capacity resulted in being to be 80 mg g^{-1} for Au^{3+} and then 70 mgl g^{-1} for Pt^{2+}. The uptake of Pt^{2+} and Au^{3+} ions on magnetite nanoparticles occurs by physico-chemical interactions, likely represented by electrostatic attractions, and the comparative adsorption magnitude is confirmed on the entire equilibrium concentration range.

A basic modelling analysis was carried out in order to determine the isotherm model that better describes the experimental data. In Table 1, Langmuir and Freundlich model parameters were reported, as derived from the regression analysis.

Table 1. Estimated parameters for the Langmuir and Freundlich models for isotherm of Pt^{2+} and Au^{3+} adsorption on Fe_3O_4 magnetite nanoparticles (T=25 °C).

	Langmuir equation			Freundlich		
	q_m mg g^{-1}	b L mmol^{-1}	r^2	k_f L^{n}mg^{1-n}g^{-1}	n	r^2
Au^{3+}	86.7	7.4563	0.9788	0.06541	0.7564	0.9955
Pt^{2+}	73.5	4.8734	0.9756	0.07645	0.8765	0.9945

The Freundlich equation frequently gives an adequate description of adsorption data over a restricted range of concentration; it is usually suitable for a highly heterogeneous surface and an adsorption isotherm lacking a plateau, indicating a multilayer adsorption[36]. Values of 1/n less than unity indicate that a significant adsorption takes place at low concentration, but the increase in the amount adsorbed with concentration becomes less significant at higher concentration and vice versa[37].

The essential characteristic of the Langmuir isotherms can be expressed in terms of a dimensionless constant separation factor or equilibrium parameter, R_L, which is defined as:

$$R_L = \frac{1}{(1 + bC_o)} \tag{7}$$

where b is the Langmuir constant and C_o is the initial metal ion concentration. The value of R_L indicates the type of isotherm to be either favourable ($0 < R_L < 1$), unfavourable ($R_L > 1$), linear ($R_L = 1$) or irreversible ($R_L = 0$). From our study, an initial metal ion concentration of 100 mg·L^{-1}, R_L values for Pt^{2+} and Au^{3+} ion adsorption ranged from 2.77 to 1.89, therefore the adsorption process is unfavourable.

As can be observed from the data reported in Table 1, the Freundlich model shows the highest comparative value of the coefficient of determination (R^2), indicating a better approximation of model parameters to the experimental counterparts. In Figure 7 the fitting of experimental data by the Langmuir model is reported.

Adsorption kinetics

In order to better analyse the rates of Pt^{2+} and Au^{3+} ion adsorption on Fe_3O_4 magnetite nanoparticles, two simple kinetic models were tested.

The pseudo-first-order rate expression, popularly known as the Lagergren equation, is generally described by the following equation[36]:

$$\frac{dq}{dt} = k_{ad}(q_e - q) \tag{8}$$

where q_e is the amount of the metal ions adsorbed at equilibrium per unit weight of sorbent (mg g^{-1}); and q is the amount of metal ions adsorbed at any time (mg g^{-1}). Additionally, k_{ad} is the rate constant (min^{-1}). Integrating with appropriate boundary conditions (q = 0 for t = 0 and q = q_t for t = t), Eq. 4 takes the form:

$$\ln(q_e - q_t) = \ln q_e - k_{ad}t \tag{9}$$

However, if the intercept does not equal the natural logarithm of equilibrium uptake of metal ions, the reaction is not likely to follow a first-order path even if experimental data have a high coefficient of determination[36]. The coefficients of determination for all metal ion adsorption kinetic tests were found to be between 0.9434 and 0.9765 and are reported in Table 2 together with the Lagergren rate constants calculated from the slope of Eq. 5 [37].

The adsorption data were also analyzed in terms of a pseudo-second-order mechanism given follow equation[35,36]:

$$\frac{dq}{dt} = k_2(q_e - q_t)^2 \tag{10}$$

where k_2 is the rate constant (mg·g^{-1}·min^{-1}). Integrating the above equation and applying boundary conditions (i.e. q = 0 for t = 0and q = q_t for t = t) gives:

$$\frac{t}{q_t} = \frac{1}{h_o} + \frac{1}{q_e}t \tag{11}$$

where h_o is the initial adsorption rate. If the second-order kinetics is applicable, the plot of t/q against t in Eq. 7 should give a linear relationship from which the constants q_e and h_o can be determined. The linear model gave a good fit to the experimental data. This means that the adsorption can be described by a pseudo-second-order rate equation, hence q_e and h_o were evaluated and are presented in Table 1. R^2 values are approximately the same for all the four metal ions, with values of about 0.999. At the limit at initial adsorption time, h_o is defined as[35-37]:

$$h_o = k_2 q_e^2 \tag{12}$$

h_o was calculated for the four metal ions and the values are reported in Table 1. The results obtained are similar to previous studies[36-37].

Table 2. Lagergren rate equation constants and pseudo second-order rate equation constants for Pt^{2+} and Au^{3+} ion adsorption on Fe_3O_4 magnetite nanoparticles.

	q_{exp}	Pseudo-first-order equation			Pseudo-second-order equation		
		q_e (mmol g^{-1})	k_1 (min^{-1})	r^2	q_e (mmol g^{-1})	k_2 (g mmol^{-1}·min^{-1})	r^2
Au^{3+}	0.0901	0.0877	0.3221	0.9687	0.0899	4.9876	0.9998
Pt^{2+}	0.0621	0.0658	0.2234	0.9754	0.0734	3.37456	0.9986

For all the regressions, the residual sum of squares (SSE), as the difference between the predicted values and the experimental data, can be calculated by the following equation:

$$\sum_n \left(q_e \exp - q_e calc\right)^2 \qquad (13)$$

where the subscripts exp and calc refer to the experimental and the calculated q values, respectively. Hence, the higher correlation coefficient (R^2) values for the pseudo-second-order kinetic model indicated that the sorption followed a pseudo-second-order mechanism, likely controlled by chemisorption.

Effect of temperature and time

For the investigated ions, adsorption experiments were conducted varying the temperature between 15 ºC and 45 ºC under the following conditions: L/S = 1:6 and pH 6.5.

Figures 9a and 9b show the curves obtained for the adsorption tests at different times and temperatures for Pt^{2+} and Au^{3+} taken as an example, respectively. As can be observed, for both ions, the adsorption capacity is greater for lower temperatures, as expected, since adsorption is an exothermic process. Moreover, the increase in adsorption capacity is higher for the lowest values of temperature.

The temperature also has an effect on the time necessary to reach the equilibrium; a higher temperature, in fact, determines a lower equilibrium time.
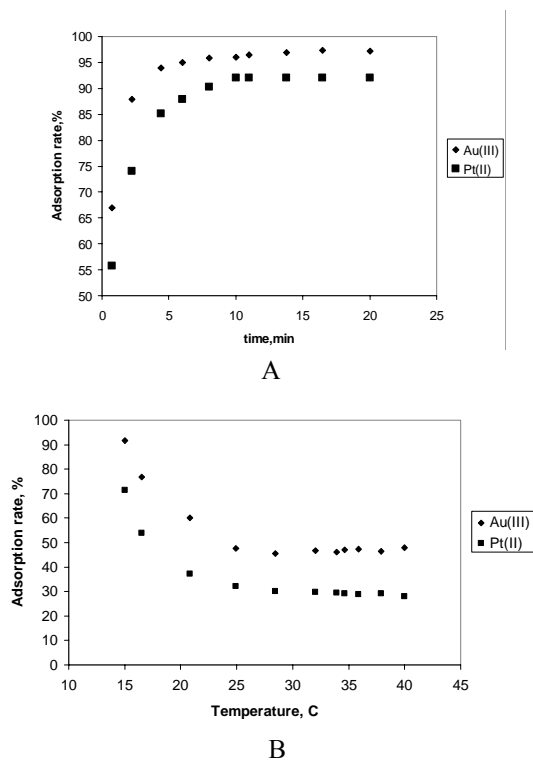

A

B

Figure 9. The effect of temperature on the adsorption of Pt^{2+} (A) and Au^{3+} (B) ions on the magnetic Fe_3O_4 nanoparticles; pH = 6.5, adsorbent dosage = 50 mg, initial metal ion concentration = 25 mg·L⁻¹.

Immersion calorimetry

This work used the technique of immersion microcalorimetry, with the aim of analysing whether the immersion of the synthesized magnetite particles in solutions studio ions generated under some correlation.

Figure 10 shows the results obtained and show that a correlation is generated between the initial concentration of each of the solutions in the range studied and the calculated enthalpy of immersion. This makes it interesting to use in studies of adsorption micro-calorimetry with such materials, since in the literature the thermodynamic variables are calculated by varying the temperature and calorimetric known from the same that this form of thermodynamic correlation is correct, produce errors which are sometimes large.
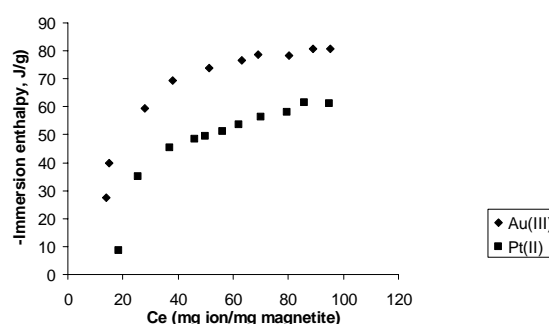

Figure 10. Immersion heats between nanoparticles of magnetite and ion solutions.

Figure 10 shows a high-energy release at low concentrations, which increases to about 60 mg L⁻¹ which then becomes constant, showing a behaviour similar to an isotherm from aqueous solution. It is interesting to note that the enthalpy values are higher between interaction Au^{3+}-magnetite for Pt^{2+}-magnetite; this is in accordance with that was found by the other techniques used by us in this work, where there is greater affinity between ions Au^{3+} and magnetite. These results open a very good possibility for thermodynamic studies using this technique.

Conclusion

In this work, Fe_3O_4 nanoparticles were synthesized by co-precipitation method and used for treating water artificially contaminated by metal ions, such as Pt^{2+} and Au^{3+}. Experimental results suggest that the adsorption capacity of Fe_3O_4 nanoparticles towards metal ions depends on the metal ions' electronegativity. The maximum adsorption capacity in the investigated conditions was 86.7 mg g⁻¹ for Au^{3+} and 76.3 mg g⁻¹ for Pt^{2+}. Moreover, adsorption capacity seems to be strongly dependent on pH solution and temperature. The adsorption mechanism seems to be mainly an electrostatic attraction between metal ions and nanoparticles influenced by the hydrated ionic radius of the metal cations. The Langmuir model interprets the adsorption data better. A kinetic analysis showed that the adsorption of all the investigated ions onto Fe_3O_4 nanoparticles occurs by a pseudo-second-order mechanism.

In conclusion, it is demonstrated here that the Fe$_3$O$_4$ nanoparticles with fine grain size (<10 nm) can be efficiently used as an effective, convenient and low-cost material for the removal and recovery of metals from wastewater. The adsorption process was found to follow the pseudo-second-order equation. The equilibrium data conformed better to Freundlich's isotherm. The immersion calorimetry technique presents a good chance to be employed in these studies and evaluates the thermodynamic variables.

References

[1] Singh, D. B., Prasad, G., Rupainwar, D. C., and Singh, V.N., *Water Air Soil Pollut.*, **1998**, *42*, 373.

[2] Jain, C. K., and Ali, I., *Water Res.*, **2000**, *34*, 4304.

[3] World Health Organization (WHO), *Environmental Health Criteria*, **2001**, 224.

[4] Benjamin, M., *Water Chemistry*, McGraw Hill, New York, **2002**.

[5] Leon, C. A., Solar, J. M., Calemma, V. and Radovic, L. R., *Carbon*, **1992**, *30*, 797.

[6] Bandosz, T. J., Jagiello, J., Contescu, C., and Schwarz, J. A., *Carbon*, **1993**, *31*, 1193.

[7] Boehm, H. P., *Carbon*, **2002**, *40*, 145.

[8] Lakatos, J., Brown, S. D., and Snape, C. E., *Fuel*, **2002**, *81*, 691.

[9] Yacoumi, S., and Tien, C., *Kinetics of Metal Ion Adsorption from Aqueous Solutions*, Kluwer Academic Publisher, Boston, **1995**.

[10] Gabaldon, C., Marzal, P., Ferrer, J., and Seco, A., *Water Res.*, **1996**, *30*, 3050.

[11] Hu, J., Lo, M., and Chen, G., *Separation and Purification Technology*, **2007**, *56*, 249.

[12] Lo Hu, J., and Chen, G., Iron-Based Magnetic Nanoparticles for Removal of Heavy Metals from Electroplating and Metal-Finishing Wastewater, In: *Nanotechnologies for Water Environment Applications*, Zhang C.T., Surampali Y.R., Lai K.C.K, Hu Z., Tyagi R.D., Lo M.C.I. (Eds.), American Society of Civil Engineers, Virginia, **2009**, 213-264.

[13] Cloete, T. E., Nanotechnology in *Water Treatment Applications*, Caister Academic Press, Norfolk, UK, **2010**.

[14] Parida, S. K., Dash, S., Patel, S., and Mishra, B. K., *Adv. Colloid Interface Sci.*, **2006**, *121*, 77.

[15] Khodabakhshi, A., Amin, M. M., and Mozaffari, M., *Iran. J. Environ. Health. Sci. Eng.*, **2011**, *8*, 189.

[16] Kang, Y. K., Risbud, S., Rabolt, J. F., and Stroeve, P., *Chem Mater.*, **1996**, *8*, 2209.

[17] Goya, G. F., Berquo, T. S., Fonseca, F. C., and Morales, M. P., *J. Appl. Phys.*, **2003**, *94*, 3520.

[18] Sudaryanto,Y., Hartono, S. B., Irawaty, W., Hindorso, H., and Ismadji, S., *Bioresour. Technol.*, **2006**, *97*, 734.

[19] Yorgun, S., Vural, N., and Demiral, H., *Microporous and Mesoporous Materials*, **2009**, *122*, 189.

[20] Wang, X., Zhao, C., Zhao, P., Dou, P., Ding, Y., and Xu, P., *Bioresource Technology*, **2009**, *100*, 2301.

[21] Sun, Y., Ma, M., Zhang, Y., and Gu, N., *Colloids and Surfaces A: Physicochem. Eng. Aspects*, **2004**, *245*, 15.

[22] Podzus, P. E., Debandi, M. V., and Daraio, M. E., *Physica B: Condensed Matter*, **2011**, *407,* 3131.

[23] Lee, D., Omolade, D., Cohen, R. E., and Rubner. M. F., *Chem. Mater.* **2007**, *19*, 1427.

[24] Thierry, B., Majewski, P., Ngothai, Y., and Shi, Y., *Int. J. of Nanotechnology*, **2007**, *4*, 523.

[25] Kocaoba, S., and Akyuz, T., *Desalination*, **2005**, *181*, 313.

[26] Giraldo, L., Huertas, J. I, Valencia, A. and Moreno J. C, *Inst Sci Technol.*, **2003**, *31*, 385.

[27] Klug, H. P., and Alexander, L. E. *X-Ray Diffraction Procedures: For Polycrystalline and Amorphous Materials,* 2nd Edition, pp. 992. Wiley-VCH, May **1974**. ISBN 0-471-49369-4.

[28] Obaid, R., Subash, C. M., and Sharif, A., *Materials Chemistry and Physics*, **2012**, *132*, 196.

[29] Meziani, M. J., Liu, P., Pathak, P., Lin, J., Vajandar, S.K., Allard, L.F., and Sun, Y.P., *Ind. Eng. Chem. Res.*, **2006**, *45*, 1539.

[30] Boistelle, R., and Astier, J. P., *J. Cryst. Growth*, **1988**, *90*, 14.

[31] Ma, M., Zhang, Y., Yu, W., Shen, H., Zhang, H., and Gu, N., *Colloids and Surfaces A: Physicochem. Eng. Aspects*, **2003**, *212*, 219.

[32] Choo, E. S. G., Tang, X. S., Sheng, Y., Shuter, B., and Xue, J., *Journal of Materials Chemistry*, **2011**, *21*, 2310.

[33] Choo, E. S. G., Yu, B., and Xue, J. M., *Journal of Colloid and Interface Science*, **2011**, *358*, 462.

[34] Hou, Y. L., Yu. H. F., and Gao, S., *J. Mater. Chem.*, **2003**, 13, 1983.

[35] Wan, S. R., Huang, J. S., Yan, H. S., and Liu, K. L., *J. Mater. Chem.*, **2006**, *16*, 298.

[36] Lagergren, S., About the Theory of So-called Adsorption of Soluble Substances, *K. Svenska Vetensk-Akad. Handl.*, **1989**, *24*, 1.

[37] Ho, Y. S., McKay, G., *Chem. Eng. J.*, **1998**, *70*, 115.